SUPPORTING INFORMATION

Conformational Dynamics of Mechanically Compliant DNA Nanostructures from Coarse-Grained Molecular Dynamics Simulations

Ze Shi,[†] Carlos E. Castro,[‡] and Gaurav Arya[*,†]

†*Department of NanoEngineering, University of California, San Diego, La Jolla, California 92093, United States*

‡*Department of Mechanical and Aerospace Engineering, The Ohio State University, Columbus, Ohio 43210, United States*

E-mail: garya@ucsd.edu

Phone: +1 (858) 822-5542. Fax: +1 (858) 534-9553

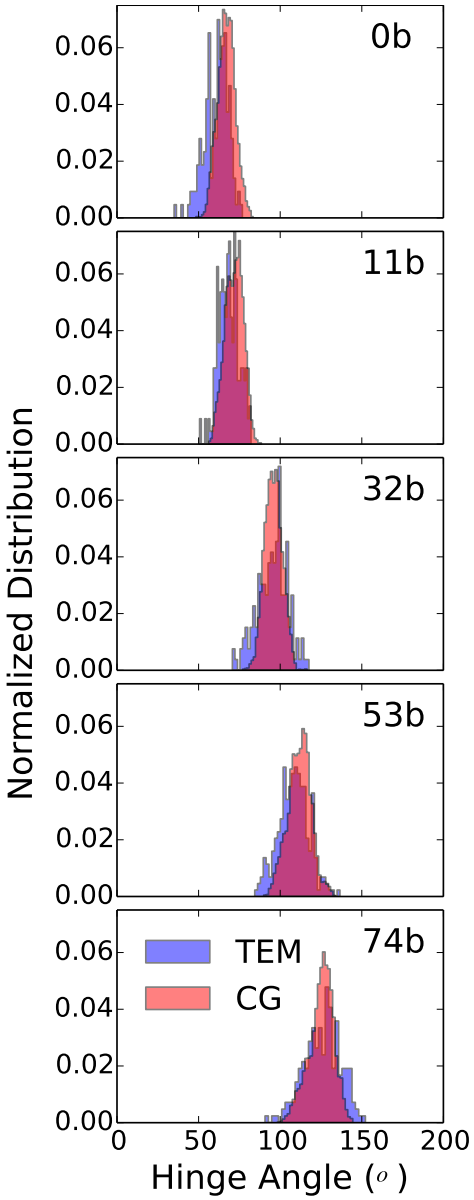

Figure S1: Normalized distributions of hinge angles Φ for the five hinge designs from CG modeling (red) and compared against those obtained from experimental TEM images (blue).

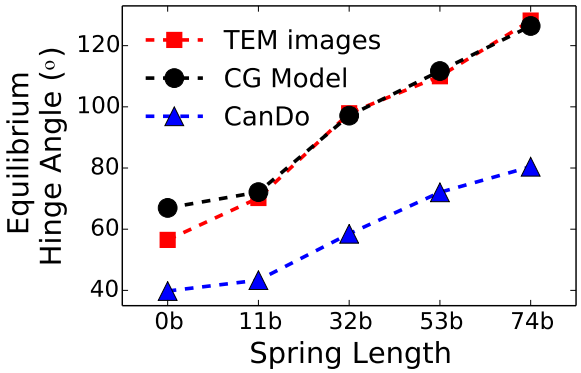

Figure S2: Equilibrium hinge angles Φ_0 for the five hinge designs predicted using the software CanDo. The angles predicted from the CG model and those obtained from experiments are shown as reference.

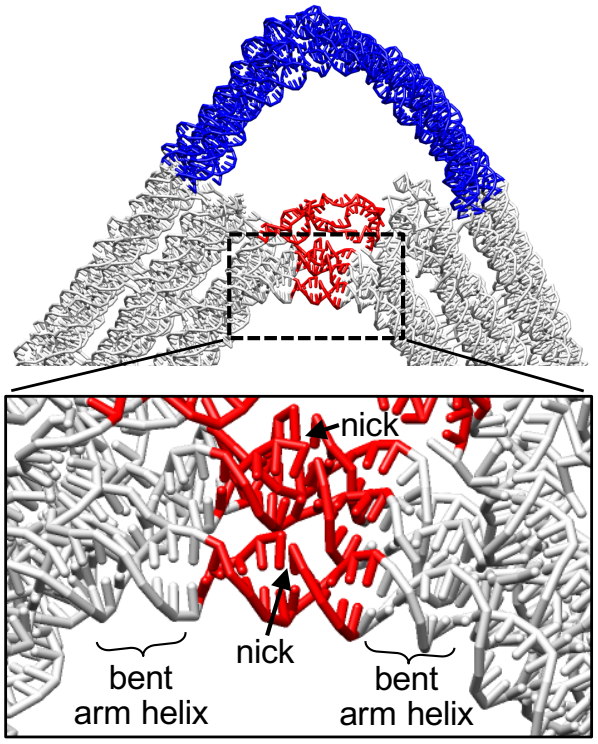

Figure S3: Representative snapshot of the joint (blue) and the springs (red) for the 0b hinge obtained from MD simulations illustrating how the three springs connecting the lower layer of hinge arm helices are effectively dsDNA helices containing single nicks and how the strong bending stress in these nicked dsDNA connections force the hinge arm helices to deform.

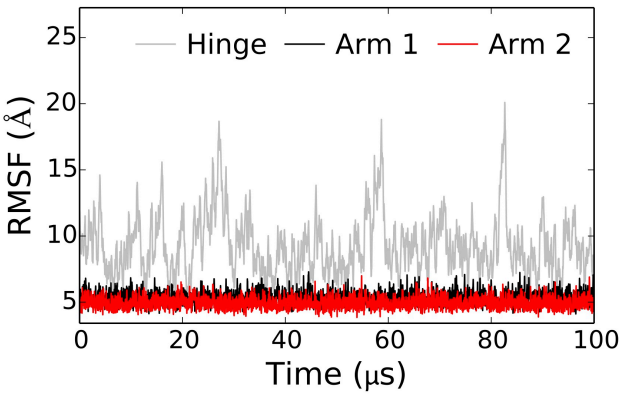

Figure S4: Root mean square fluctuations (RMSF) of the entire 0b hinge and of its two arms individually. The RMSFs are calculated relative to the average structures obtained over the entire MD trajectory.

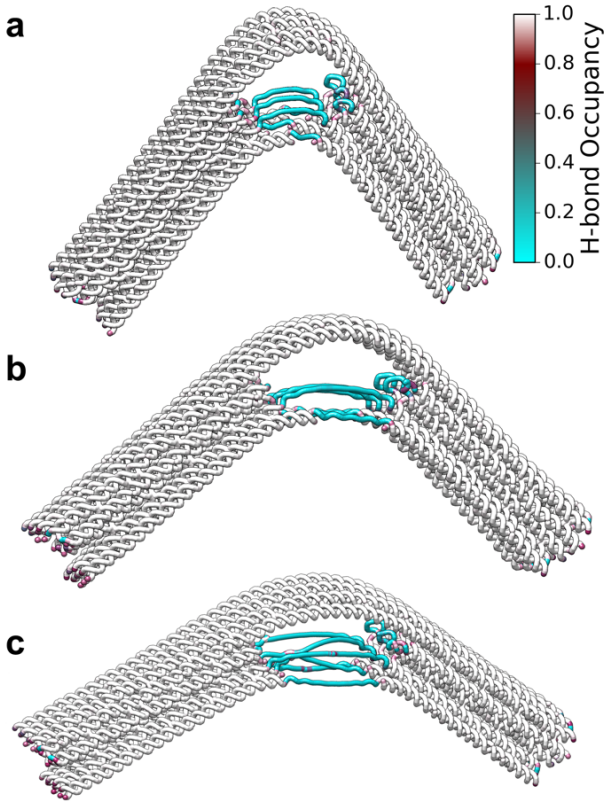

Figure S5: DNA-backbone representation of (a) 11b, (b) 32b, and (c) 53b hinges, colored according to the fraction of the time their nucleotide bases remain bonded to their complementary bases (H-bond occupancy). Cyan-, red-, and white-colored regions indicate unpaired, weakly paired, and strong paired bases.

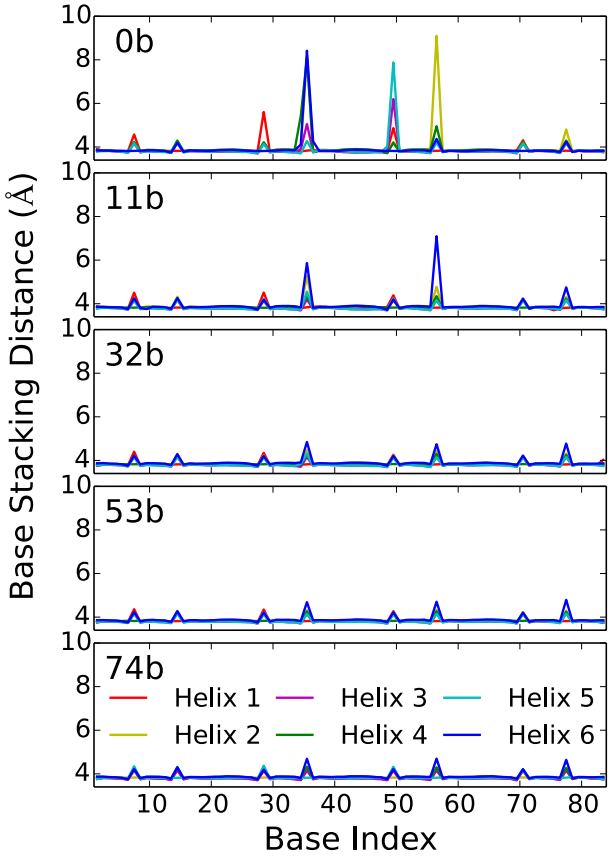

Figure S6: Distance between adjacent bases of the staple strands of the six joint helices, plotted for each of the five hinge designs.

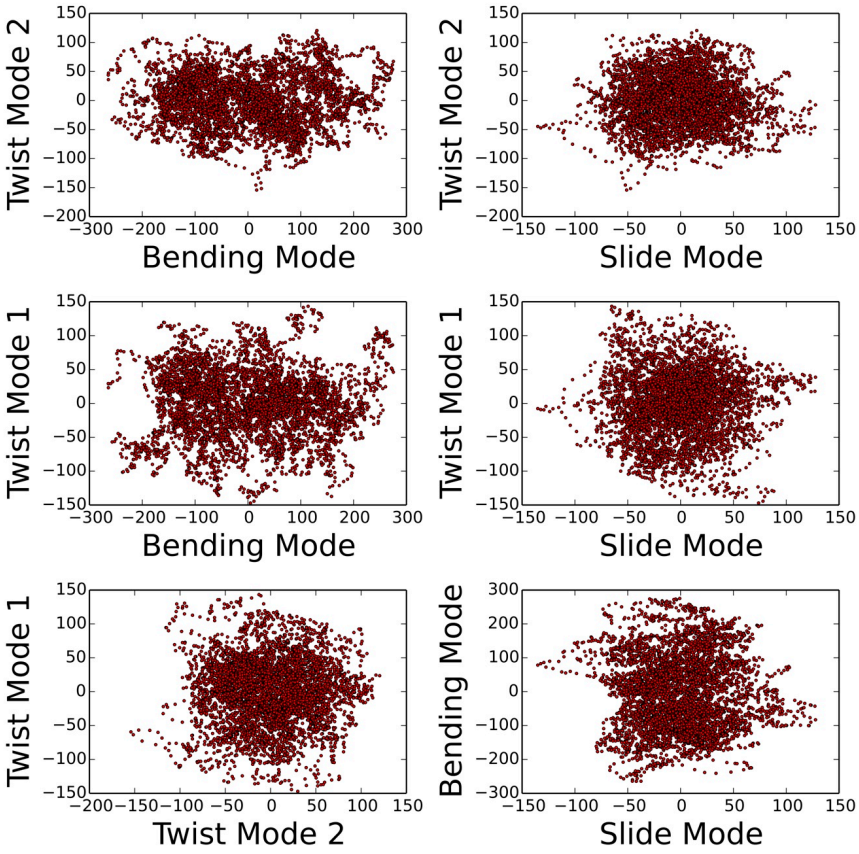

Figure S7: Correlation between the four largest dynamic modes of the 74b hinge obtained from principal component analysis. The x- and y-axes show the magnitude of the projections.

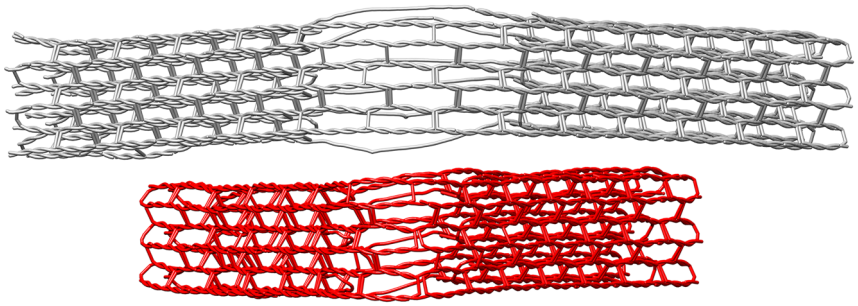

Figure S8: Average structure of the 74b (top) and 0b hinge (bottom) depicting the expulsion of the ssDNA springs in the former due to electrostatic repulsion. Hinges are represented by lines connecting the center of masses of the DNA bases and only their top view is shown.

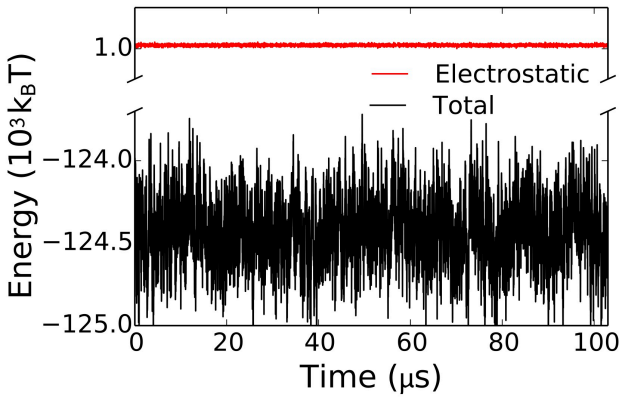

Figure S9: Total potential energy and the component of this energy arising purely from electrostatic repulsion plotted as a function of simulation time for the 0b hinge.

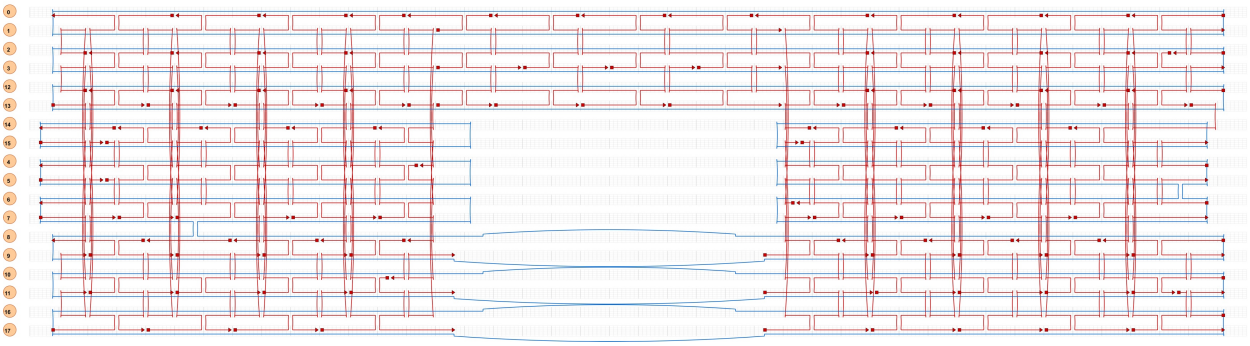

Figure S10: caDNAno design of the 0b hinge. The ssDNA scaffold and staple strands are shown in blue and red, respectively. The dsDNA helices are labeled 0 to 17 on the left.

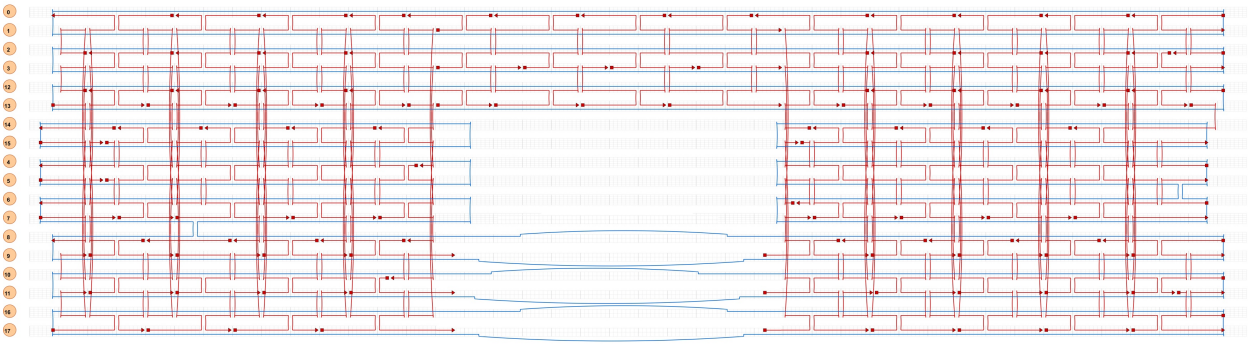

Figure S11: caDNAno design of the 11b hinge. The ssDNA scaffold and staple strands are shown in blue and red, respectively. The dsDNA helices are labeled 0 to 17 on the left.

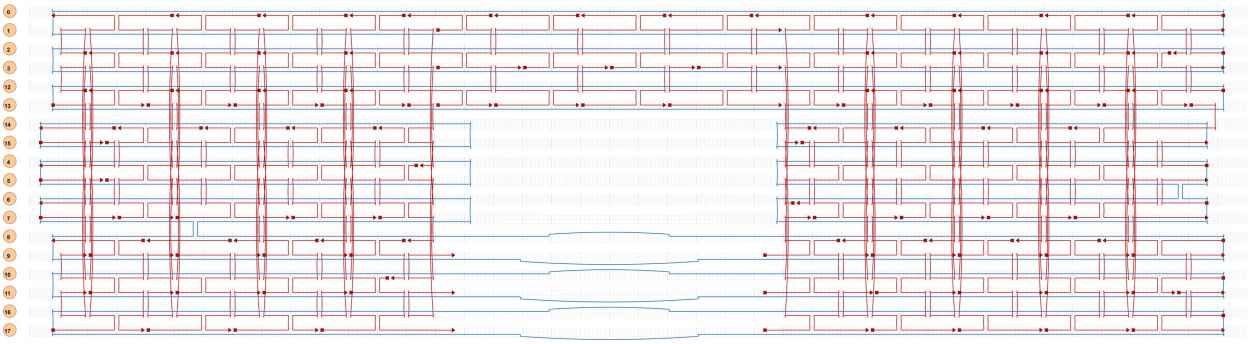

Figure S12: caDNAno design of the 32b hinge. The ssDNA scaffold and staple strands are shown in blue and red, respectively. The dsDNA helices are labeled 0 to 17 on the left.

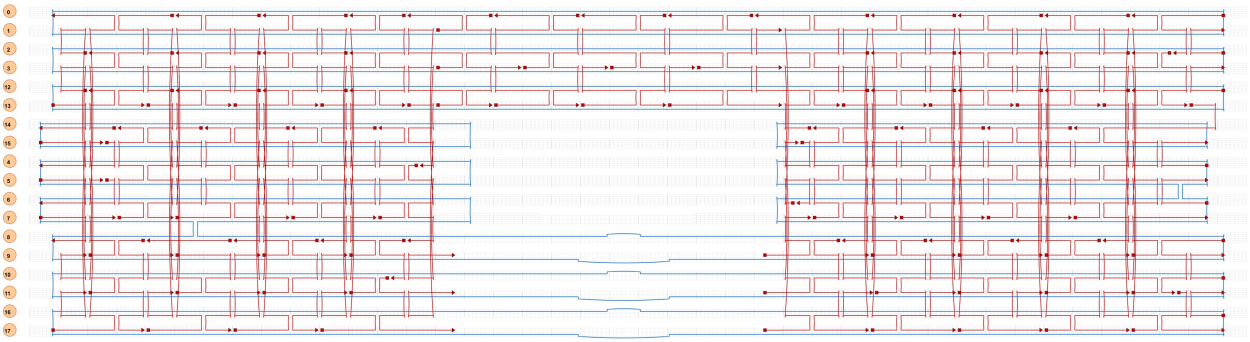

Figure S13: caDNAno design of the 53b hinge. The ssDNA scaffold and staple strands are shown in blue and red, respectively. The dsDNA helices are labeled 0 to 17 on the left.

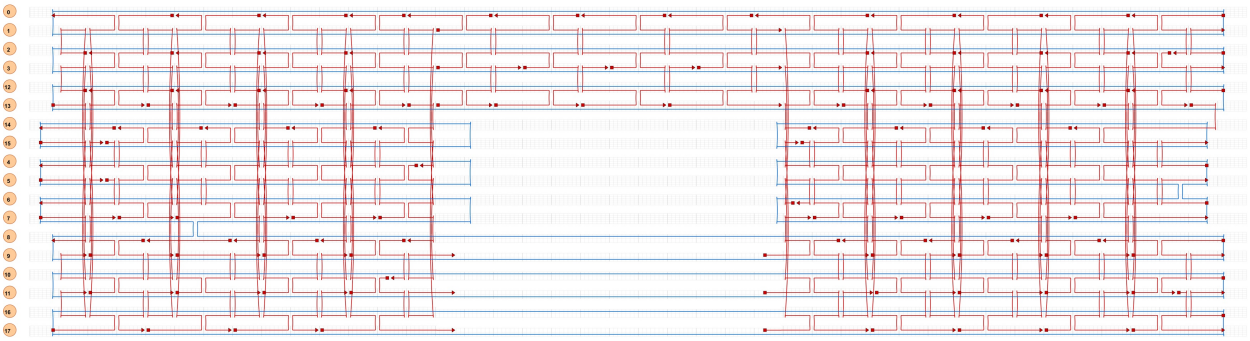

Figure S14: caDNAno design of the 74b hinge. The ssDNA scaffold and staple strands are shown in blue and red, respectively. The dsDNA helices are labeled 0 to 17 on the left.

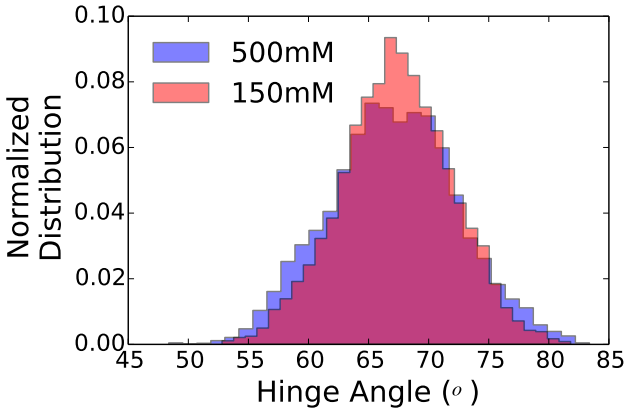

Figure S15: Hinge angle distribution of the 0b hinge obtained from CG MD simulations at two different monovalent salt concentrations: 150 mM (red) and 500 mM (blue).

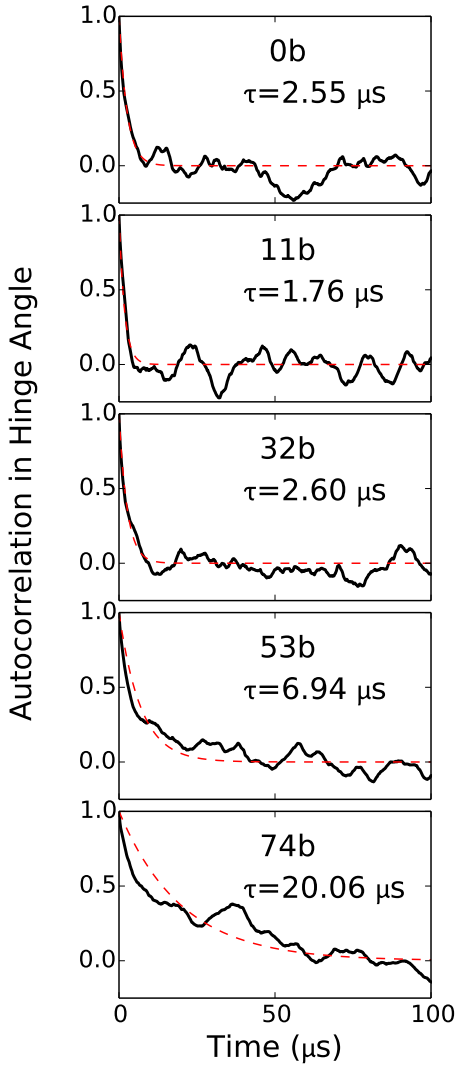

Figure S16: Autocorrelations $\langle(\Phi(t)-\Phi_0)(\Phi(0)-\Phi_0)\rangle$ in the hinge angle computed from CG MD simulations for the five hinge designs (solid black lines) along with exponential fits to the decaying portion of the curves (dashed red lines). The characteristic decay time constants obtained from the fits are also specified in each figure.